Effective Elastic Stiffness for Periodic Masonry Structures via Eigenstrain Homogenization

Gang Wang[1]; Shaofan Li[2]; Hoang-Nam Nguyen[3]; and Nicholas Sitar, M.ASCE[4]

Abstract: The equivalent periodic eigenstrain method is used to evaluate the effective elastic stiffness of periodic masonry structure. An Eshelby tensor, for a unit cell of the periodic masonry structure, is derived analytically, and is combined with a strain energy approach to formulate the effective stiffness of the masonry. The new homogenization scheme is simple, one step, and closed form. The model described the periodicity and microstructure details of brick and mortar precisely and is compared to other analytical models. The improved accuracy of model prediction is validated through a finite-element simulation reported in literature.

DOI: 10.1061/(ASCE)0899-1561(2007)19:3(269)

CE Database subject headings: Elasticity; Stiffness; Masonry; Finite elements.

Introduction

Masonry is a two-phase material comprised of brick and mortar joints, normally arranged periodically. Studying the in-plane load deformation characteristics of the masonry is important for designing and retrofitting masonry structures. As a viable alternative to otherwise expensive and time-consuming laboratory and field experiments, numerical and analytical methods have attracted extensive attention in both industry and the research community.

One of the most comprehensive approaches is to model each brick and each mortar joint in the assembly, where linear and nonlinear constitutive behaviors of bricks and mortar can be considered. Although detailed stress–strain and failure mechanism are well studied, methods of this category demand intensive computational efforts and usually rely on the expertise of finite element technique (for example, in Gambarotta and Lagomarsino 1997; Michel et al. 1999; Giambanco et al. 2001; Formica et al. 2002). The representation of each brick and each joint is essentially impractical for modeling a real large masonry structure, so this approach is only suitable to simulate a small specimen or a representative unit. The overall property of masonry can be derived accordingly from the numerical experiments (Ma et al. 2001).

[1]Graduate Researcher, Dept. of Civil and Environmental Engineering, Univ. of California, Berkeley, CA 94720.

[2]Associate Professor, Dept. of Civil and Environmental Engineering, Univ. of California, Berkeley, CA 94720 (corresponding author). E-mail: li@ce.berkeley.edu

[3]Staff Engineer, Ball Aerospace & Technologies Corp., Systems Engineering Solutions, 2201 Buena Vista SE, Albuquerque, NM 87106; formerly, Graduate Student, Dept. of Civil and Environmental Engineering, Univ. of California, Berkeley, CA 94720.

[4]Professor, Dept. of Civil and Environmental Engineering, Univ. of California, Berkeley, CA 94720.

Note. Associate Editor: Jason Weiss. Discussion open until August 1, 2007. Separate discussions must be submitted for individual papers. To extend the closing date by one month, a written request must be filed with the ASCE Managing Editor. The manuscript for this paper was submitted for review and possible publication on January 13, 2004; approved on March 7, 2006. This paper is part of the ***Journal of Materials in Civil Engineering***, Vol. 19, No. 3, March 1, 2007. ©ASCE, ISSN 0899-1561/2007/3-269–277/$25.00.

On the other hand, masonry can be treated as an effectively elastic continuum. The overall property can be homogenized analytically or semianalytically. For example, Pande et al. (1989) proposed a multilayer model to estimate the effective elastic stiffness for the brick–mortar system. Based on the strain energy approach, the equivalent properties of a multilayered system with alternating joints are obtained in closed form. The mutilayer solution is first applied to homogenize the horizontal strip comprised of brick units and vertical head joints, and then used again to integrate the above homogenized strips with the horizontal bed joints, as schematically illustrated in Fig. 1(b). Pietruszczak and Niu (1992) also proposed a two-step homogenization scheme. In the first step, they assumed that brick units form a homogeneous matrix uniformly interspersed with aligned head joints as inclusions. The equivalent stiffness of the medium can be found using Eshelby's solution for an elliptic cylinder inclusion in combination with the Mori–Tanaka mean field theory (Mori and Tanaka 1973), as was initially reported by Zhao and Weng (1990) for ribbon-reinforced composites. Then the homogenized medium from the first step and the continuous bed joints form a laminate structure whose effective stiffness is found using mechanics of the laminate material. The scheme is also illustrated in Fig. 1(c).

As pointed out by other researchers, one of the drawbacks of these "two-step" homogenizations is that the result depends on the step order. Besides, the bond pattern of brick and mortar (e.g., stacked bond versus running bond) cannot be distinguished in their models. To overcome these difficulties, one-step approaches have been pursued. For example, a one-step homogenization by Anthoine (1995) has rigorously prescribed the periodic boundary conditions. Unfortunately, due to the complexity of the masonry unit cell, it has to be used in conjunction with the finite-element method, so it is semianalytical in nature. Recently, the asymptotic homogenization method has also been used and combined with the finite-element method (Cecchi and Rizzi 2001). However, the method is too computationally intensive. To be fully analytical, Bati et al. (1999) proposed using aligned elliptical cylinders to approximate the rectangular bricks, as shown in Fig. 1(d). In this model, the Zhao and Weng (1990) solution and the Mori–Tanaka mean field theory are applied, which is very similar to the first step of Pietruszczak and Niu (1992) discussed above except that the brick units, instead of the head joints, are treated as inclusions

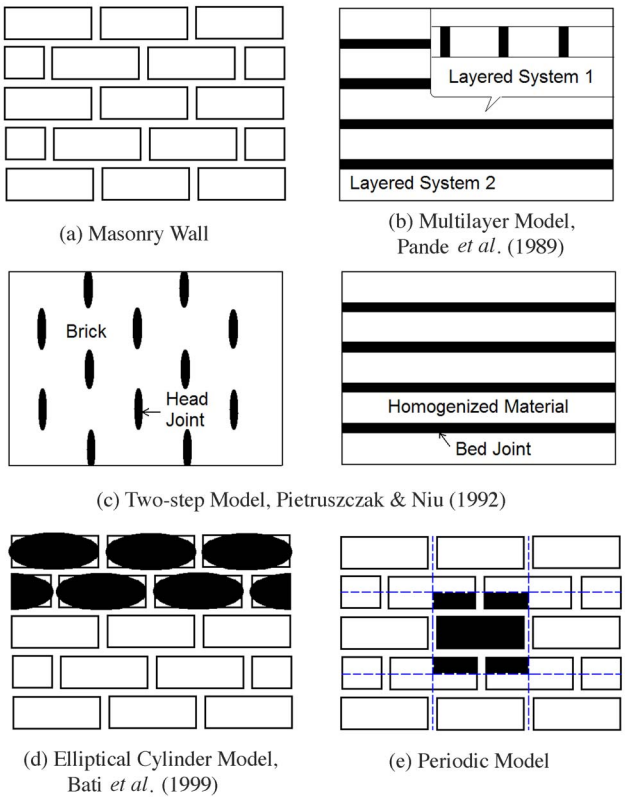

(a) Masonry Wall

(b) Multilayer Model, Pande *et al*. (1989)

(c) Two-step Model, Pietruszczak & Niu (1992)

(d) Elliptical Cylinder Model, Bati *et al*. (1999)

(e) Periodic Model

Fig. 1. Homogenization models for masonry structure

embedded in the matrix of mortar. It is also noted that the concentration of brick inclusions is very high in this model. The plausibility of the elliptical cylinder model has been experimentally validated against experimental results.

However, in view of these analytical models [Figs. 1(b–d)], neither of them have explicitly taken into account the specific pattern of brick and mortar, nor have fully exploited the periodicity of geometry, stress, strains, as well as other field quantities. In this paper, the writers propose implementing a micromechanical homogenization technique, the so-called periodic eigenstrain homogenization method, to model masonry structures. In this method, the periodicity of field quantities is enforced by Fourier series, and a periodic unit area will be studied in which the microstructural details of the bricks (inclusions) and mortar (matrix) can be accurately described [see Fig. 1(e)]. A similar scheme was initiated by Nemat-Nasser et al. (1982) for periodically distributed inclusions of spherical and cylindrical geometries, and was applied to composite materials by Luciano and Barbero (1994). However, it has never been implemented in periodic masonry homogenization. In this paper, we first introduce the concept of unit cell and the periodic eigenstrain homogenization. The Eshelby tensor for the unit cell is then derived to relate the disturbance field with the eigenstrain field, which plays the same role as the Eshelby tensor for an inclusion in an infinite space (Eshelby 1957). Then we derive the effective material properties of the masonry structure based on a strain energy approach. The new homogenization scheme appears to be simple, one step, and closed form. Numerical application is provided in the last section, and the model is compared to other analytical models and validated by a finite-element simulation reported in the literature.

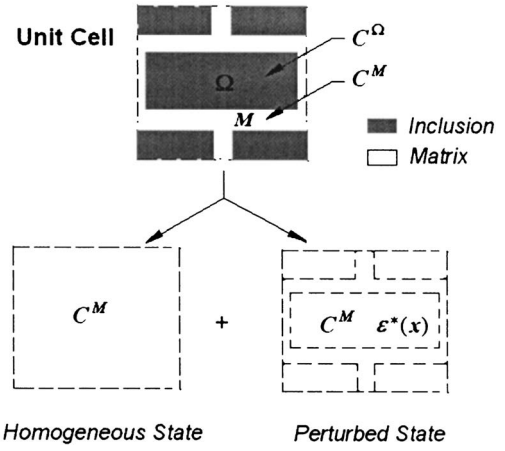

Fig. 2. Decomposition of microstructured unit cell

Periodic Eigenstrain Formulation

Unit Cell

For the periodic masonry structure, a unit area (called *unit cell*) is highlighted in Fig. 1(e), which represents the unit of periodicity in the horizontal and vertical directions. There are, of course, other possible choices for the unit cell.

The unit cell (V) is a microstructured composite. Illustrated in Fig. 2, it contains one complete brick unit, four one-quarter-sized brick units, and mortar joints between the bricks. In our analysis, the brick units are considered to be inclusions (Ω) and mortar is treated as matrix (M). We denote $\mathbf{C}^{\Omega}$ and $\mathbf{C}^{M}$ as the stiffness of the inclusion and matrix. Accordingly, $\mathbf{D}^{\Omega}$ and $\mathbf{D}^{M}$ are reserved for the compliance of the inclusion and matrix.

The unit cell is conceptually different from the representative volume element (RVE) that is often used in micromechanical homogenization methods. The RVE contains a large number of inclusions such that it can *statistically* represent the overall composite properties. Correspondingly, the inclusion distribution in the RVE can only be accounted for in a statistically uniform manner, whereas for the unit cell, the microstructure can be described *exactly*. Moreover, since the unit cell is a periodic unit in the periodic structure, it prompts us to use the Fourier series to represent the disturbance fields, which can be solved analytically, as will be demonstrated in the following sections.

Stress–Strain in Unit Cell

Assume a displacement field, $\mathbf{u}^0$, is prescribed on the boundary of the unit cell. The displacement field will induce a constant strain field $\boldsymbol{\varepsilon}^0$ in a homogeneous material, i.e.

$$\mathbf{u}^0 = \mathbf{x} \cdot \boldsymbol{\varepsilon}^0 \tag{1}$$

Due to the presence of inclusions, the total strain $\boldsymbol{\varepsilon}$ within the unit cell is the addition of the constant strain $\boldsymbol{\varepsilon}^0$ prescribed and a disturbance strain field $\boldsymbol{\varepsilon}^d(\mathbf{x})$, which is unknown at present and to be determined later. Assuming both inclusions and matrix are linearly elastic, the total stress in the inhomogeneous unit cell is

$$\boldsymbol{\sigma}(\mathbf{x}) = \begin{cases} \mathbf{C}^{M}:[\boldsymbol{\varepsilon}^{o} + \boldsymbol{\varepsilon}^{d}(\mathbf{x})], & \mathbf{x} \in M \\ \mathbf{C}^{\Omega}:[\boldsymbol{\varepsilon}^{o} + \boldsymbol{\varepsilon}^{d}(\mathbf{x})], & \mathbf{x} \in \Omega \end{cases} \tag{2}$$

If the inclusions are replaced by the matrix properties, the inhomogeneous unit cell can be decomposed as the superposition of

two states: a homogeneous state and a perturbed state, as is schematically illustrated in Fig. 2. To equivalently account for the presence of the second phase (inclusion), an equivalent eigenstrain field, ε^*_{ij}, is introduced, which would produce a compatible deformation field without generating stresses. The stress consistency condition requires that

$$\sigma_{ij}(\mathbf{x}) = \begin{cases} C^{\Omega}_{ijkl}[\varepsilon^0_{kl} + \varepsilon^d_{kl}(\mathbf{x})] = C^M_{ijkl}[\varepsilon^0_{kl} + \varepsilon^d_{kl}(\mathbf{x}) - \varepsilon^*_{kl}(\mathbf{x})], & \mathbf{x} \in \Omega \quad (3a) \\ C^M_{ijkl}[\varepsilon^0_{kl} + \varepsilon^d_{kl}(\mathbf{x})], & \mathbf{x} \in M \quad (3b) \end{cases}$$

Note that the eigenstrain is only prescribed on the inclusion in Eq. (3). We can extend the definition of the eigenstrain to the whole unit cell V as

$$\varepsilon^*_{ij}(\mathbf{x}) = \begin{cases} \varepsilon^*_{ij}(\mathbf{x}), & \mathbf{x} \in \Omega \\ 0, & \mathbf{x} \in M \end{cases} \tag{4}$$

so Eq. (3) can be rewritten in a unified fashion over V

$$\sigma_{ij}(\mathbf{x}) = C^M_{ijkl}[\varepsilon^0_{kl} + \varepsilon^d_{kl}(\mathbf{x}) - \varepsilon^*_{kl}(\mathbf{x})], \quad \mathbf{x} \in V \tag{5}$$

Assuming no body force, the stresses satisfy the following equilibrium condition

$$\sigma_{ij,j}(\mathbf{x}) = C^M_{ijkl}[\varepsilon^0_{kl} + \varepsilon^d_{kl}(\mathbf{x}) - \varepsilon^*_{kl}(\mathbf{x})]_{,j} = 0, \quad \mathbf{x} \in V \tag{6}$$

Relation between Eigenstrain and Perturbed Strain

For a self-contained presentation, we first outline the periodic eigenstrain formulation (Nemat-Nasser et al. 1982) for solids with periodic structures. Since masonry has a periodic structure, the disturbance displacement field and eigenstrain field are also periodic. We can express these periodic fields using the Fourier series. The disturbance displacement field can be written as

$$u^d_i(\mathbf{x}) = \sum_{\boldsymbol{\xi} \in \Lambda'} \hat{u}^d_i(\boldsymbol{\xi}) \exp(i\boldsymbol{\xi} \cdot \mathbf{x}) \tag{7a}$$

$$\hat{u}^d_i(\boldsymbol{\xi}) = \frac{1}{V} \int_V u^d_i(\mathbf{x}) \exp(-i\boldsymbol{\xi} \cdot \mathbf{x}) d\mathbf{x} \tag{7b}$$

where V=area of the unit cell; and the symbol $i = \sqrt{-1}$.

Similarly, the periodic eigenstrain field can be expressed as

$$\varepsilon^*_{kl}(\mathbf{x}) = \sum_{\boldsymbol{\xi} \in \Lambda'} \hat{\varepsilon}^*_{kl}(\boldsymbol{\xi}) \exp(i\boldsymbol{\xi} \cdot \mathbf{x}) \tag{8a}$$

$$\hat{\varepsilon}^*_{kl}(\boldsymbol{\xi}) = \frac{1}{V} \int_V \varepsilon^*_{kl}(\mathbf{x}) \exp(-i\boldsymbol{\xi} \cdot \mathbf{x}) d\mathbf{x} \tag{8b}$$

Notice that the summation of the infinite Fourier series is made on the set

$$\Lambda' = \left\{ \boldsymbol{\xi} = \xi_1 \mathbf{e}_1 + \xi_2 \mathbf{e}_2 \;\middle|\; \xi_1 = \frac{n_1 \pi}{L},\ \xi_2 = \frac{n_2 \pi}{H};\ n_1, n_2 = 0, \pm 1, \pm 2 \ldots ; n_1^2 + n_2^2 \neq 0 \right\}$$

in which $2L$ and $2H$=length and height of the unit cell, respectively.

From Eq. (7*a*), the disturbance strain field is found as

$$\varepsilon^d_{ij}(\mathbf{x}) = \frac{1}{2}[u^d_{i,j}(\mathbf{x}) + u^d_{j,i}(\mathbf{x})] = \frac{i}{2} \sum_{\boldsymbol{\xi} \in \Lambda'} [\xi_i \hat{u}^d_j(\boldsymbol{\xi}) + \xi_j \hat{u}^d_i(\boldsymbol{\xi})] \exp(i\boldsymbol{\xi} \cdot \mathbf{x}) \tag{9}$$

Substituting Eqs. (8) and (9) into Eq. (6), we have

$$-C^M_{ijkl} \hat{u}^d_k(\boldsymbol{\xi}) \xi_l \xi_j = i C^M_{ijkl} \hat{\varepsilon}^*_{kl}(\boldsymbol{\xi}) \xi_j \tag{10}$$

Inverting the above equation

$$\hat{u}^d_i(\boldsymbol{\xi}) = -i \frac{N_{ik}(\boldsymbol{\xi})}{D(\boldsymbol{\xi})} C^M_{klmn} \hat{\varepsilon}^*_{mn}(\boldsymbol{\xi}) \xi_l \tag{11}$$

where

$$N_{ik}(\boldsymbol{\xi}) = 1/2 e_{imn} e_{kpq} K_{mp} K_{nq}; \quad K_{ik}(\boldsymbol{\xi}) = C^M_{ijkl} \xi_l \xi_j$$

$$D(\boldsymbol{\xi}) = e_{mnl} K_{m1} K_{n2} K_{l3}$$

and

$$e_{ijk} = \text{permutation symbol } (i,j,k = 1,2,3) \tag{12}$$

Combining Eqs. (9) and (11), we get

$$\begin{aligned} \varepsilon^d_{ij}(\mathbf{x}) &= \sum_{\boldsymbol{\xi} \in \Lambda'} \frac{1}{2} \left[\xi_i \xi_l \frac{N_{jk}(\boldsymbol{\xi})}{D(\boldsymbol{\xi})} C^M_{klmn} + \xi_j \xi_l \frac{N_{ik}(\boldsymbol{\xi})}{D(\boldsymbol{\xi})} C^M_{klmn} \right] \\ &\quad \times \hat{\varepsilon}^*_{mn}(\boldsymbol{\xi}) \exp(i\boldsymbol{\xi} \cdot \mathbf{x}) \\ &= \sum_{\boldsymbol{\xi} \in \Lambda'} g_{ijmn}(\boldsymbol{\xi}) \hat{\varepsilon}^*_{mn}(\boldsymbol{\xi}) \exp(i\boldsymbol{\xi} \cdot \mathbf{x}) \end{aligned} \tag{13}$$

in which

$$g_{ijmn}(\boldsymbol{\xi}) = \frac{1}{2} \left[\xi_i \xi_l \frac{N_{jk}(\boldsymbol{\xi})}{D(\boldsymbol{\xi})} C^M_{klmn} + \xi_j \xi_l \frac{N_{ik}(\boldsymbol{\xi})}{D(\boldsymbol{\xi})} C^M_{klmn} \right]$$

If both matrix and inclusion are isotropic materials, then

$$\begin{aligned} g_{ijmn}(\boldsymbol{\xi}) &= \frac{1}{2\xi^2} [\xi_j(\delta_{in}\xi_m + \delta_{im}\xi_n) + \xi_i(\delta_{jn}\xi_m + \delta_{jm}\xi_n)] \\ &\quad - \frac{1}{1-\nu} \frac{\xi_i \xi_j \xi_m \xi_n}{\xi^4} + \frac{\nu}{1-\nu} \frac{\xi_i \xi_j}{\xi^2} \delta_{mn} \end{aligned} \tag{14}$$

where $\xi^2 = \xi_k \xi_k = \xi_1^2 + \xi_2^2$, and ν=Poisson's ratio of the matrix.

Now, substituting Eq. (8*b*) into Eq. (13), the disturbance strain field can be written as an integral function of the eigenstrain

$$\varepsilon^d_{ij}(\mathbf{x}) = \frac{1}{V} \sum_{\boldsymbol{\xi} \in \Lambda'} g_{ijmn}(\boldsymbol{\xi}) \int_\Omega \varepsilon^*_{mn}(\mathbf{x}') \exp(-i\boldsymbol{\xi} \cdot \mathbf{x}') d\mathbf{x}' \exp(i\boldsymbol{\xi} \cdot \mathbf{x}) \tag{15}$$

Eq. (15) relates the disturbance strain field with prescribed eigenstrain. Moreover, we can rewrite stress consistent condition Eq. (3a) in tensor form as follows

$$\boldsymbol{\varepsilon}^d = \mathbf{A}^{\Omega} : \boldsymbol{\varepsilon}^* - \boldsymbol{\varepsilon}^0 \tag{16}$$

in which $\mathbf{A}^{\Omega} = (\mathbf{C}^M - \mathbf{C}^{\Omega})^{-1} : \mathbf{C}^M$.

Substituting Eq. (16) into Eq. (15) yields

$$\begin{aligned} &\varepsilon^0_{ij}(\mathbf{x}) - A^{\Omega}_{ijmn} \varepsilon^*_{mn}(\mathbf{x}) + \sum_{\boldsymbol{\xi} \in \Lambda'} g_{ijmn}(\boldsymbol{\xi}) \\ &\quad \times \frac{1}{V} \int_\Omega \varepsilon^*_{mn}(\mathbf{x}') \exp(-i\boldsymbol{\xi} \cdot \mathbf{x}') d\mathbf{x}' \exp(i\boldsymbol{\xi} \cdot \mathbf{x}) = 0 \end{aligned} \tag{17}$$

Eq. (17) relates the eigenstrain $\boldsymbol{\varepsilon}^*$ to the prescribed constant strain $\boldsymbol{\varepsilon}^0$. Since it is difficult to solve it exactly, we shall take the average of Eq. (17) over the inclusion, Ω, as

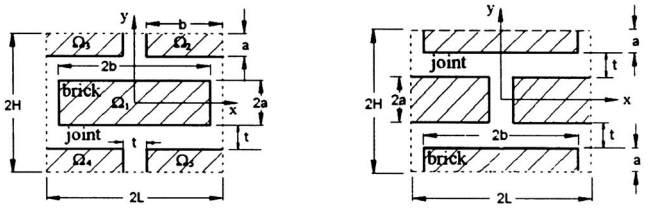

(a) Example 1 (b) Example 2

Fig. 3. Unit cells for running bond masonry

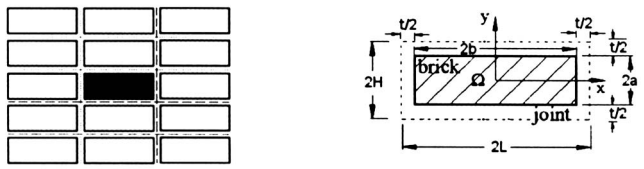

(a) Masonry Wall (b) Unit Cell

Fig. 4. Unit cells for stack bond masonry

$$\varepsilon_{ij}^0 - A_{ijmn}^{\Omega}\bar{\varepsilon}_{mn}^* + \sum_{\boldsymbol{\xi}\in\Lambda'} g_{ijmn}(\boldsymbol{\xi})\frac{1}{V}\int_{\Omega}\varepsilon_{mn}^*(\mathbf{x}') \times\exp(-i\boldsymbol{\xi}\cdot\mathbf{x}')d\mathbf{x}'\left[\frac{1}{\Omega}\int_{\Omega}\exp(i\boldsymbol{\xi}\cdot\mathbf{x})d\mathbf{x}\right] = 0 \quad (18)$$

In order to simplify the above expression, define

$$g_0(\boldsymbol{\xi}) = \frac{1}{\Omega}\int_{\Omega}\exp(i\boldsymbol{\xi}\cdot\mathbf{x})d\mathbf{x} \quad (19)$$

We further approximate $\varepsilon_{mn}^*(\mathbf{x}')$ with its volume average $\bar{\varepsilon}_{mn}^*$, i.e., $\varepsilon_{mn}^*(\mathbf{x}') \approx \bar{\varepsilon}_{mn}^*$; thus Eq. (18) can be reduced to

$$\varepsilon_{ij}^0 = A_{ijmn}^{\Omega}\bar{\varepsilon}_{mn}^* - \sum_{\boldsymbol{\xi}\in\Lambda'} g_{ijmn}(\boldsymbol{\xi})g_0(\boldsymbol{\xi})\bar{\varepsilon}_{mn}^* \cdot \frac{\Omega}{V}\frac{1}{\Omega}\int_{\Omega}\exp(-\boldsymbol{\xi}\cdot\mathbf{x}')d\mathbf{x}'$$
$$= A_{ijmn}^{\Omega}\bar{\varepsilon}_{mn}^* - \sum_{\boldsymbol{\xi}\in\Lambda'} f_{\Omega}\cdot g_{ijmn}(\boldsymbol{\xi})g_0(-\boldsymbol{\xi})\bar{\varepsilon}_{mn}^* \quad (20)$$

where $f_{\Omega}=\Omega/V=$volume fraction of inclusions inside the unit cell. Comparing Eq. (16) to Eq. (20), the relationship between the disturbance strain field and the eigenstrain field is found to be

$$\varepsilon_{ij}^d = \sum_{\boldsymbol{\xi}\in\Lambda'} f_{\Omega}\cdot g_0(\boldsymbol{\xi})g_0(-\boldsymbol{\xi})g_{ijmn}(\boldsymbol{\xi})\bar{\varepsilon}_{mn}^* = S_{ijmn}^{\Omega}\bar{\varepsilon}_{mn}^* \quad (21)$$

and Eshelby tensor for the periodic unit cell is determined as

$$S_{ijmn}^{\Omega} = \sum_{\boldsymbol{\xi}\in\Lambda'} f_{\Omega}\cdot g_0(\boldsymbol{\xi})g_0(-\boldsymbol{\xi})g_{ijmn}(\boldsymbol{\xi}) \quad (22)$$

which plays the same role as the Eshelby tensor for an inclusion in an *infinite* space (Eshelby 1957). However, the tensor we obtained here is for the unit cell, which is finite in size. The tensor conveys the microstructure details of matrix and inclusion within the unit cell and it is represented by an infinite series.

Evaluation of Eshelby Tensor

Now we proceed to evaluate the Eshelby tensor Eq. (22). Consider the unit cell for running bond masonry shown in Fig. 3(a), which has the dimension of $2H$ and $2L$. The height and length of one brick unit are $2a$ and $2b$, respectively. Evaluate the integral over the domain of inclusions directly

$$g_0(\xi) = \frac{1}{\Omega}\int_{\Omega}\exp(i\boldsymbol{\xi}\cdot\mathbf{x})d\mathbf{x}$$
$$= \sum_{r=1}^{5}\int_{\Omega_r}\exp(i\boldsymbol{\xi}\cdot\mathbf{x}')d\mathbf{x}'$$
$$= \int_{-a}^{a}\int_{-b}^{b}\exp(i\xi_1x_1' + i\xi_2x_2')dx_1'\,dx_2'$$
$$+ \int_{H-a}^{H}\int_{L-b}^{L}\exp(i\xi_1x_1' + i\xi_2x_2')dx_1'\,dx_2'$$
$$+ \int_{H-a}^{H}\int_{-L}^{-L+b}\exp(i\xi_1x_1' + i\xi_2x_2')dx_1'\,dx_2'$$
$$+ \int_{-H}^{-H+a}\int_{-L}^{-L+b}\exp(i\xi_1x_1' + i\xi_2x_2')dx_1'\,dx_2'$$
$$+ \int_{-H}^{-H+a}\int_{L-b}^{L}\exp(i\xi_1x_1' + i\xi_2x_2')dx_1'\,dx_2' \quad (23)$$

After some algebra, the above equation can be evaluated explicitly as

$$g_0(\boldsymbol{\xi}) = \frac{1}{2ab}\frac{1}{\xi_1\xi_2}(\sin(\xi_1b)\sin(\xi_2a) + \{\sin(\xi_1L) - \sin[\xi_1(L-b)]\}\cdot\{\sin(\xi_2H) - \sin[\xi_2(H-a)]\}) \quad (24)$$

$g_0(\boldsymbol{\xi})$ contains the microstructure details of inclusions and matrix in this unit cell. As mentioned before, the choice of unit cell is not unique, and the expression for $g_0(\boldsymbol{\xi})$ would be different for another unit cell. For example, an alternative unit cell can be chosen as illustrated in Fig. 3(b) for the same running bond masonry. Correspondingly, $g_0(\boldsymbol{\xi})$ can be evaluated as

$$g_0(\boldsymbol{\xi}) = \frac{1}{2ab}\frac{1}{\xi_1\xi_2}(\sin(\xi_2a)\{\sin(\xi_1L) - \sin[\xi_1(L-b)]\} + \sin(\xi_1b) \times\{\sin(\xi_2H) - \sin[\xi_2(H-a)]\}) \quad (25)$$

It should be worth pointing out here that our procedure *does not* depend on the choice of the unit cell. One can verify that Eqs. (24) and (25) yield identical results if used in an ensuing homogenization scheme.

For the stack bond masonry shown in Fig. 4(a), the unit cell can be chosen as Fig. 4(b), with all geometry defined. Correspondingly

$$g_0(\boldsymbol{\xi}) = \frac{1}{ab}\frac{1}{\xi_1\xi_2}\sin(\xi_1 b)\sin(\xi_2 a) \tag{26}$$

Due to symmetry of the unit cell, $g_0(\boldsymbol{\xi})$ is an even function, i.e.

$$g_0(\boldsymbol{\xi}) = g_0(-\boldsymbol{\xi}) \tag{27}$$

An explicit expression for the Eshelby tensor can be obtained by substituting Eqs. (24), (26), and (27) into Eq. (22)

$$\begin{aligned} S^{\Omega}_{ijmn} &= \sum_{\boldsymbol{\xi}\in\Lambda'} f_{\Omega}\cdot g_0(\boldsymbol{\xi})g_0(-\boldsymbol{\xi})g_{ijmn}(\boldsymbol{\xi}) \\ &= \sum_{\boldsymbol{\xi}\in\Lambda'} f_{\Omega}\cdot[g_0(\boldsymbol{\xi})]^2\left\{\frac{1}{2\xi^2}[\xi_j(\delta_{in}\xi_m+\delta_{im}\xi_n) \right. \\ &\left. + \xi_i(\delta_{jn}\xi_m+\delta_{jm}\xi_n)] - \frac{1}{1-\nu}\frac{\xi_i\xi_j\xi_m\xi_n}{\xi^4} + \frac{\nu}{1-\nu}\frac{\xi_i\xi_j}{\xi^2}\delta_{mn}\right\} \end{aligned} \tag{28}$$

To facilitate implementation, all components of the Eshelby tensor are listed in the Appendix. The convergence property of the infinite series is also studied there. For a given unit cell, the infinite series can be evaluated once and for all, and the numerical results can be used in various applications.

Effective Stiffness of Mansonry

To obtain the effective stiffness tensor of masonry, we adopt the strain energy approach proposed by Nemat-Nasser et al. (1982).

First, define an averaging operator

$$\langle\cdot\rangle_V = \frac{1}{V}\int_V \cdot\, dV \tag{29}$$

Under the prescribed displacement condition Eq. (1), it is easy to prove that the averaged total strain equals the constant strain, i.e., $\langle\boldsymbol{\varepsilon}\rangle_{\mathbf{V}}=\boldsymbol{\varepsilon}^0$, and the averaged disturbance strain vanishes, i.e., $\langle\boldsymbol{\varepsilon}^{\mathbf{d}}\rangle_{\mathbf{V}}=0$. Hence the total strain energy per unit cell (V) can be computed as

$$\begin{aligned} W &= \frac{1}{2}\int_V \sigma_{ij}\varepsilon_{ij}dV \\ &= \frac{1}{2}\int_V C^M_{ijkl}(\varepsilon^0_{kl}+\varepsilon^d_{kl}-\varepsilon^*_{kl})(\varepsilon^0_{ij}+\varepsilon^d_{ij})dV \\ &= \frac{1}{2}\int_V C^M_{ijkl}\varepsilon^0_{ij}\varepsilon^0_{kl}dV - \frac{1}{2}\int_V C^M_{ijkl}\varepsilon^0_{ij}\varepsilon^*_{kl}dV \end{aligned} \tag{30}$$

On the other hand, let $\mathbf{C}^h$ be the homogenized effective stiffness tensor. The effective stress–strain relation for the averaged stress and strain can be written as

$$\langle\boldsymbol{\sigma}\rangle_V = \mathbf{C}^h:\langle\boldsymbol{\varepsilon}\rangle_V = \mathbf{C}^h:\boldsymbol{\varepsilon}^0 \tag{31}$$

So the total strain energy per unit cell (V) can be written alternatively as

$$W = \frac{1}{2}\int_V \langle\boldsymbol{\sigma}\rangle_V:\langle\boldsymbol{\varepsilon}\rangle_V dV = \frac{1}{2}\int_V C^h_{ijkl}\varepsilon^0_{ij}\varepsilon^0_{kl}dV \tag{32}$$

Comparing Eq. (30) and (32), we obtained

$$C^h_{ijkl}\varepsilon^0_{ij}\varepsilon^0_{kl} = C^M_{ijkl}\varepsilon^0_{ij}\varepsilon^0_{kl} - f_{\Omega}C^M_{ijkl}\varepsilon^0_{ij}\bar{\varepsilon}^*_{kl} \tag{33}$$

Now we seek to estimate the effective stiffness $\mathbf{C}^h$. Recalling that

$$\boldsymbol{\varepsilon}^0 = \mathbf{A}^{\Omega}:\bar{\boldsymbol{\varepsilon}}^* - \boldsymbol{\varepsilon}^d = (\mathbf{A}^{\Omega}-\mathbf{S}^{\Omega}):\bar{\boldsymbol{\varepsilon}}^* \tag{34}$$

in which $\mathbf{A}^{\Omega}=(\mathbf{C}^M-\mathbf{C}^{\Omega})^{-1}:\mathbf{C}^M$, we finally obtained the effective stiffness of the masonry as

$$\mathbf{C}^h = \mathbf{C}^M:[\mathbf{1}^{(4S)} - f_{\Omega}(\mathbf{A}^{\Omega}-\mathbf{S}^{\Omega})^{-1}] \tag{35}$$

where $\mathbf{1}^{(4S)}$=forth-order identity tensor; and f_{Ω}=volume fraction of inclusions. Similarly, the effective compliance is exactly the inverse of the above,

$$\mathbf{D}^h = \mathbf{D}^M:[\mathbf{1}^{(4S)} - f_{\Omega}(\mathbf{A}^{\Omega}-\mathbf{S}^{\Omega})^{-1}] \tag{36}$$

The resulting effective modulus is simple and analytical.

Numerical Application

To illustrate the plausibility of the proposed periodic eigenstrain method, a numerical example is considered in this section. The brick and mortar are assumed to be isotropic. The Young's modulus of the brick (E_b) and Poisson's ratio (ν_b) are 11,000 MPa and 0.20, respectively. The ratio of Young's moduli of the brick over the mortar (E_b/E_m) ranges from 1.1 to 11, and Poisson's ratio for the mortar (ν_m) is 0.25. The brick dimensions are 250 (length) $\times$ 55 mm (height).

Considering the plane stress case, the elastic stiffness of the mortar, the brick unit and masonry can be written in matrix notation

$$[\mathbf{C}^M] = \begin{bmatrix} C^m_{11} & C^m_{12} & 0 \\ C^m_{21} & C^m_{22} & 0 \\ 0 & 0 & C^m_{33} \end{bmatrix} = \frac{E_m}{(1-\nu_m^2)}\begin{bmatrix} 1 & \nu_m & 0 \\ \nu_m & 1 & 0 \\ 0 & 0 & (1-\nu_m)/2 \end{bmatrix} \tag{37}$$

$$[\mathbf{C}^b] = \begin{bmatrix} C^b_{11} & C^b_{12} & 0 \\ C^b_{21} & C^b_{22} & 0 \\ 0 & 0 & C^b_{33} \end{bmatrix} = \frac{E_b}{(1-\nu_b^2)}\begin{bmatrix} 1 & \nu_b & 0 \\ \nu_b & 1 & 0 \\ 0 & 0 & (1-\nu_b)/2 \end{bmatrix} \tag{38}$$

$$[\mathbf{C}^h] = \begin{bmatrix} C^h_{11} & C^h_{12} & 0 \\ C^h_{21} & C^h_{22} & 0 \\ 0 & 0 & C^h_{33} \end{bmatrix} \tag{39}$$

After numerical evaluation, the Eshelby tensor can also be presented in matrix form as

$$[\mathbf{S}^{\Omega}] = \begin{bmatrix} S^{\Omega}_{1111} & S^{\Omega}_{1122} & 0 \\ S^{\Omega}_{2211} & S^{\Omega}_{2222} & 0 \\ 0 & 0 & 2S^{\Omega}_{1212} \end{bmatrix} \tag{40}$$

The effective stiffness matrix for the masonry $\mathbf{C}^h$ can be easily computed from Eq. (35). In Fig. 5, the ratios of effective stiffness $\mathbf{C}^h$ over the brick stiffness $\mathbf{C}^b$ are plotted against the mortar thickness t and the brick–mortar stiffness ratio E_b/E_m for each nonzero component. The mortar stiffness and thickness have significant effects on the overall properties of masonry. Moreover, all curves start from unity and asymptotically approach their theoretical limits (C^m_{ij}/C^b_{ij}) as the thickness of mortar joints increases.

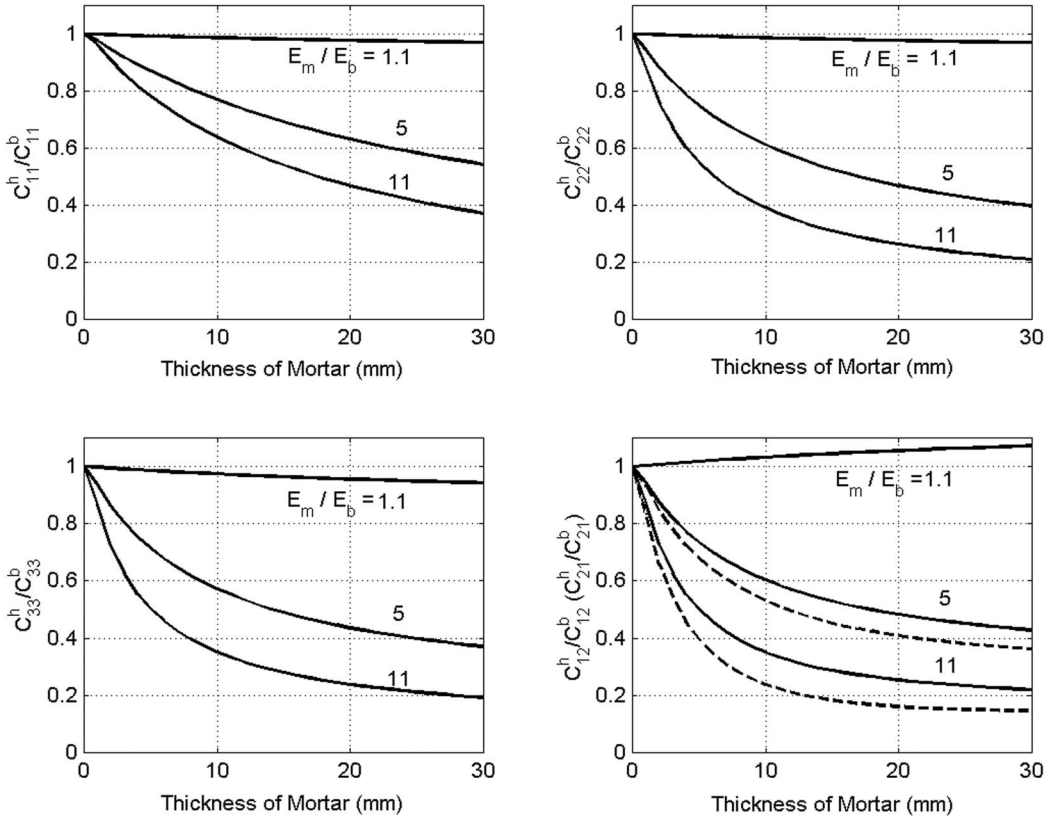

Fig. 5. Ratios between components of effective masonry stiffness (C^h) and brick stiffness (C^b) for running bond

It is also interesting to point out that the resulting effective stiffness matrix of the masonry is not symmetric. In other words, the masonry composite is not exactly orthotropic. This property stems from the fact that the Eshelby tensor matrix is not symmetric in general, i.e., $S^{\Omega}_{1122} \neq S^{\Omega}_{2211}$. The ratio of C^h_{12}/C^b_{12} is plotted in the dashed lines against C^h_{21}/C^b_{21} in solid lines in Fig. 5, in which differences between these two components are evident, especially for the cases of high stiffness ratios. The finding is consistent with the finite-element results presented by Ma et al. (2001). This feature also distinguishes our proposed model from most other models reported in the literature, where orthotropy of masonry stiffness is usually assumed as a priori. In principle, the masonry composite should not be exactly orthotropic unless the RVE is infinitely large.

The periodic model is further compared to three other analytical methods, namely, the multilayer method (Pande et al. 1989), two-step method (Pietruszczak and Niu 1992), and elliptical cylinder model (Bati et al. 1999). The procedure of each method has been briefly described in the "Introduction." Fig. 6 shows a comparison of each component. In general, all these methods produce quite consistent predictions, although considerable discrepancies appear in C^h_{11} and C^h_{12} components. All approaches give similar results when the stiffness ratio E_b/E_m is close to unity.

For further comparison, the Young's modulus of the mortar is set to be 2,200 MPa, and the head and bed mortar joints are 10 mm thick, with all other parameters remaining unchanged. This example has been numerically simulated by Anthoine (1995) using a linear finite-element method (FEM) program with periodic boundary conditions. The numerical results together with those predicted by the analytical models are summarized in Table 1. Four effective properties of the masonry are given for comparison: the Young's moduli in horizontal and vertical directions (E_1 and E_2), Poisson's ratio v_{12} and shear modulus G_{12}. All methods produce results comparable to the finite element solution. Although both the brick and mortar are isotropic, a marked anisotropy of the overall property is captured by all methods, which is highlighted in the difference between the Young's moduli (E_1 and E_2) and the low value of the shear modulus G_{12}. The largest error is found in the two-step method (Pietruszczak and Niu 1992), whereas the proposed periodic model gives the best overall prediction, followed by the multilayer method (Pande et al. 1989). It is also worth pointing out that the bond pattern is found to have negligible influence, as shown in the first two rows of Table 1. The periodic model corroborates the finite-element results for both bond patterns, and remarkably, even the subtleties between these two patterns are well captured. As discussed before, all other methods cannot make a distinction for the different bond patterns.

Conclusions

The periodic eigenstrain method and a strain energy approach have been used in a homogenization procedure to estimate the effective stiffness of masonry. The periodic model is a one-step homogenization scheme, which fully exploits the exact microstructure details of brick and mortar, and the periodicity of the masonry. The proposed method results in a simple, closed-form, analytical model to provide engineers with a convenient tool to evaluate the effective material properties for masonry.

The results obtained in the proposed method have been compared to other popular analytical methods, such as the multilayer model (Pande et al. 1989), the two-step model (Pietruszczak and Niu 1992), and the elliptical cylinder model (Bati et al. 1999) as

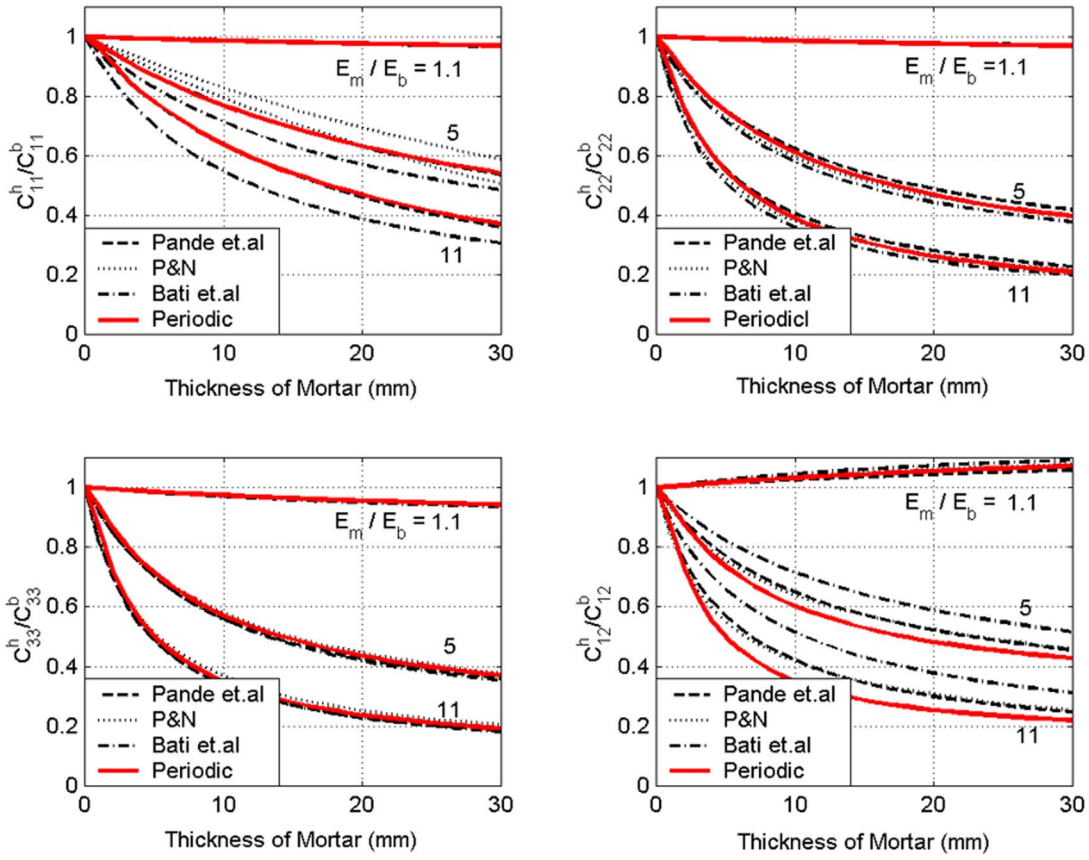

Fig. 6. Comparison between periodic model and other models

well as a finite-element simulation. The results demonstrate that the periodic model provides improved accuracy and the implementation remains very simple. Although the bond pattern was found to have little influence on the overall elastic properties in our example, the subtlety can be captured well by the periodic model. Nevertheless, bond patterns may significantly influence the crack formation and the damage mode in the nonlinear range, as was observed in the laboratory tests.

Limitations of the analytical models should be recognized. Perfect bonding between mortar and brick is usually assumed, and there is no allowance for slipping, separation, and cracking of the joints and bricks. Moreover, the mortar and brick materials are assumed linearly elastic to facilitate analytical derivation. Compared to the experimental measurements, analytical models may overpredict the effective stiffness since defects in fabrication and construction are always expected.

Acknowledgments

The writers would like to acknowledge the financial support from Pacific Earthquake Engineering Research (PEER) Center under the NSF Award No. EEC-9701568 and National Science Foundation NSF Grant No. CMS-0239130.

Appendix. Eshelby Tensor for Periodic Masonry Structure

Eshelby tensor for periodic masonry is a fourth-order tensor that can be numerically evaluated from the following infinite series:

$$S^{\Omega}_{ijmn} = \sum_{\xi \in \Lambda'} f_{\Omega} \cdot g_0(\xi) g_0(-\xi) g_{ijmn}(\xi) \tag{41}$$

Complete expressions for each component are listed

Table 1. Effective Elastic Constants of Masonry Structure

Methods of homogenization	E_1 (MPa)	E_2 (MPa)	ν_{12}	G_{12} (MPa)
FEM, stack bond (Anthoine 1995)	8,530	6,790	0.196	2,580
FEM, running bond (Anthoine 1995)	8,620	6,770	0.200	2,620
Periodic model, stack bond	8,568	6,850	0.191	2,594
Periodic model, running bond	8,574	6,809	0.197	2,620
Multilayer method (Pande et al. 1989)	8,525	6,906	0.208	2,569
Two-step method (Pietruszczak and Niu 1992)	9,187	6,588	0.215	2,658
Elliptical cylinder model (Bati et al. 1999)	7,784	6,315	0.247	2,556

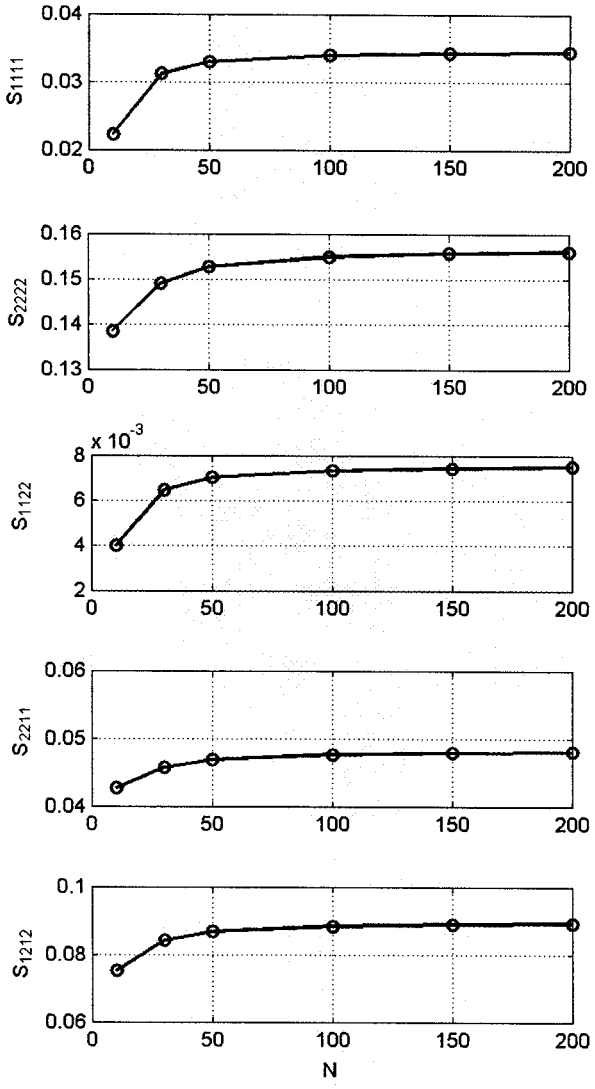

Fig. 7. Convergence of the components of Eshelby tensor

$$S^{\Omega}_{1111} = \sum_{\boldsymbol{\xi}\in\Lambda'} f_{\Omega}\cdot[g_0(\boldsymbol{\xi})]^2\cdot\left(\frac{2-\nu}{1-\nu}\frac{\xi_1^2}{\xi^2}-\frac{1}{1-\nu}\frac{\xi_1^4}{\xi^4}\right)$$

$$S^{\Omega}_{2222} = \sum_{\boldsymbol{\xi}\in\Lambda'} f_{\Omega}\cdot[g_0(\boldsymbol{\xi})]^2\cdot\left(\frac{2-\nu}{1-\nu}\frac{\xi_2^2}{\xi^2}-\frac{1}{1-\nu}\frac{\xi_2^4}{\xi^4}\right)$$

$$S^{\Omega}_{1122} = \sum_{\boldsymbol{\xi}\in\Lambda'} f_{\Omega}\cdot[g_0(\boldsymbol{\xi})]^2\cdot\left(\frac{\nu}{1-\nu}\frac{\xi_1^2}{\xi^2}-\frac{1}{1-\nu}\frac{\xi_1^2\xi_2^2}{\xi^4}\right)$$

$$S^{\Omega}_{2211} = \sum_{\boldsymbol{\xi}\in\Lambda'} f_{\Omega}\cdot[g_0(\boldsymbol{\xi})]^2\cdot\left(\frac{\nu}{1-\nu}\frac{\xi_2^2}{\xi^2}-\frac{1}{1-\nu}\frac{\xi_1^2\xi_2^2}{\xi^4}\right)$$

$$S^{\Omega}_{1212} = \sum_{\boldsymbol{\xi}\in\Lambda'} f_{\Omega}\cdot[g_0(\boldsymbol{\xi})]^2\cdot\left(\frac{1}{2}-\frac{1}{1-\nu}\frac{\xi_1^2\xi_2^2}{\xi^4}\right)$$

$$S^{\Omega}_{2121} = S^{\Omega}_{2112} = S^{\Omega}_{1221} = S^{\Omega}_{1212} \tag{42}$$

where f_{Ω}=volume fraction of the brick; ν=Poisson's ratio of the mortar; $\xi^2=\xi_1^2+\xi_2^2$; and $g_0(\boldsymbol{\xi})$=function of bond geometry.

For running bond

$$g_0(\boldsymbol{\xi}) = \frac{1}{2ab}\frac{1}{\xi_1\xi_2}(\sin(\xi_1 b)\sin(\xi_2 a) + \{\sin(\xi_1 L)-\sin[\xi_1(L-b)]\}\cdot\{\sin(\xi_2 H)-\sin[\xi_2(H-a)]\}) \tag{43}$$

For stack bond

$$g_0(\boldsymbol{\xi}) = \frac{1}{ab}\frac{1}{\xi_1\xi_2}\sin(\xi_1 b)\sin(\xi_2 a) \tag{44}$$

All other components, $S^{\Omega}_{1112}, S^{\Omega}_{1121}, S^{\Omega}_{2212}, S^{\Omega}_{2221}, S^{\Omega}_{1211}, S^{\Omega}_{1222}, S^{\Omega}_{2111}, S^{\Omega}_{2122}$ are zeros due to antisymmetry. The summations are made on the set

$$\Lambda' = \left\{ \boldsymbol{\xi}=\xi_1\mathbf{e}_1+\xi_2\mathbf{e}_2 \;\middle|\; \begin{array}{l} \xi_1=\dfrac{n_1\pi}{L}, \xi_2=\dfrac{n_2\pi}{H} \\ n_1,n_2=0,\pm1,\pm2\ldots;n_1^2+n_2^2\neq 0 \end{array} \right\} \tag{45}$$

where $2L$ and $2H$=dimensions of the unit cell (see Figs. 3 and 4).

In numerical evaluation, the infinite series needs to be truncated to finite terms, i.e.

$$S^{\Omega}_{ijmn} = \sum_{n_1=-N}^{N}{}' \sum_{n_2=-N}^{N}{}' f_{\Omega}\cdot[g_0(\boldsymbol{\xi})]^2\cdot g_{ijmn}(\boldsymbol{\xi}) \tag{46}$$

where a prime on Σ indicates that $n_1^2+n_2^2=0$ is excluded in the summation. For $n_1=0$ or $n_2=0$, Eqs. (43) or (44) should take its value at the zero limit, which is simple and finite.

Fig. 7 shows an example for each component computed against N. It shows a strong convergence profile for all components. Usually, $N=50$ gives satisfactory results (2–3% error), and it is used throughout in our reported analysis.

References

Anthoine, A. (1995). "Derivation of the in-plane elastic characteristics of masonry through homogenization theory." *Int. J. Solids Struct.*, 32(20), 137–163.

Bati, S. B., Ranocchiai, G., and Rovero, L. (1999). "Suitability of micromechnical model for elastic analysis of masonry." *J. Eng. Mech.*, 125(8), 922–929.

Cecchi, A., and Rizzi, N. L. (2001). "Heterogeneous elastic solids: a mixed homogenization-rigidification technique." *Int. J. Solids Struct.*, 38, 29–36.

Eshelby, J. D. (1957). "The determination of the elastic field of an ellipsoidal inclusion, and related problems." *Proc. R. Soc. London, Ser. A*, 241, 376–396.

Formica, G., Sansalone, V., and Casciaro, R. (2002) "A mixed solution strategy for the nonlinear analysis of brick masonry walls." *Comput. Methods Appl. Mech. Eng.*, 191, 5847–5876.

Gambarotta, G., and Lagomarsino, S. (1997) "Damage models for the seismic response of brick masonry shear walls. Part I: The mortar joint model and its applications." *Earthquake Eng. Struct. Dyn.*, 26, 423–439.

Giambanco, G., Rizzo, S., and Spallino, R. (2001) "Numerical analysis of masonry structures via interface models." *Comput. Methods Appl. Mech. Eng.*, 190, 6493–6511.

Luciano, R., and Barbero, E. J. (1994). "Formulas for the stiffness of composites with periodic microstructure." *Int. J. Solids Struct.*, 31(21), 2933–2944.

Ma, G., Hao, H., and Lu, Y. (2001). "Homogenization of masonry using

numerical simulations." *J. Eng. Mech.*, 127(5), 421–431.
Michel, J. C., Moulinec, H., and Suquet, P. (1999) "Effective properties of composite materials with periodic microstructure: A computational approach." *Comput. Methods Appl. Mech. Eng.*, 172, 109–143.
Mori, T., and Tanaka, K. (1973). "Average stress in the matrix and average elastic energy of materials with misfitting inclusions." *Acta Metall.*, 21, 571–574.
Nemat-Nasser, S., Iwakuma, T., and Hejazi, M. (1982). "On composites with periodic structure." *Mech. Mater.*, 1, 239–267.
Pande, G. N., Liang, J. X., and Middleton, J. (1989). "Equivalent elastic moduli for brick masonry." *Comput. Geotech.*, 8, 243–265.
Pietruszczak, S., and Niu, X. (1992). "A mathematical description of macroscopic behavior of brick masonry." *Int. J. Solids Struct.*, 29(5), 531–546.
Zhao, Y. H., and Weng, G. J. (1990). "Effective elastic moduli of ribbon-reinforced composites." *J. Appl. Mech.*, 57(1), 158–167.